Journal of Computational Applied Mechanics 2026, 57(2): 275-295

DOI: 10.22059/jcamech.2026.408914.1751

RESEARCH PAPER

Investigation of Darcy-Forchheimer Magnetohydrodynamic Casson Fluid Flow over a Nonlinear Permeable Stretching Sheet with Temperature-Reliant Viscosity

Dhananjay Yadav [1, *], Hajar Al Nasiri [1], Mukesh Kumar Awasthi [2], Pushap Lata Sharma [3], Zahrah Al Wahibi [1], Mana Al Saadi [1], Muzna Al Riyami [1], Alzahraa Al Toubi [1], Balqis Al Jabri [1]

[1]*Department of Mathematical & Physical Sciences, University of Nizwa, Oman*
[2]*Department of Mathematics, Babasaheb Bhimrao Ambedkar University, Lucknow 226025, India*
[3]*Department of Mathematics & Statistics, Himachal Pradesh University, Summer Hill, Shimla, 171005, India*

Abstract

This examination numerically inspects the influences of key factors on the flow and heat transmission of a Casson fluid over a nonlinearly stretching sheet in a permeable medium, considering inconstant viscosity and a magnetic field. The boundary-layer equations were cracked applying the Runge–Kutta technique, with results confirmed by MATLAB's bvp5c solver and validated against published data. Results show that velocity rises with higher Prandtl number and the nonlinear factor of the stretching sheet but drops with higher porosity factor, Forchheimer number, Casson factor, magnetic field factor, and viscosity variation factor. Temperature declines with Prandtl number and the nonlinear factor of the stretching sheet but enlargements with other parameters. The nonlinear factor of the stretching sheet boosts skin friction and heat transmission, whereas higher porosity factor, Forchheimer number, viscosity variation factor, magnetic field factor, and Casson factor lessen them. The findings offer insight into the mutual effects of non-Newtonian performance, magnetic field, and permeable media on boundary layer flow and thermal transportation.

Keywords: Nonlinear stretching sheet; Casson fluid; Darcy–Forchheimer permeable medium; MHD; viscosity deviation

1. Introduction

The inspection of non-Newtonian fluid mechanism has lately gained major importance because of its widespread industrial and technological applications in the fields of polymer processing, biomedical structures, oil recovery, and industrialization of materials [1-4]. Amongst numerous non-Newtonian models, the Casson fluid model is mainly useful since it clarifies the rheological behavior of yield-stress fluids such as blood, honey, and printing inks. Unlike the Newtonian fluid, the Casson fluid exhibitions twofold behavior: below a critical yield stress, the Casson fluid acts like an elastic solid, which, after crossing the critical stress, becomes a viscous fluid [5-8]. Therefore, their flow features under innumerable physical influences are of primary interest regarding the enrichment in the efficiency and stability of the pertinent industrial processes. Awais et al. [9] analyzed the thermo-

* Corresponding author. *E-mail address:* dhananjayadav@gmail.com; dhananjay@unizwa.edu.om

physical properties of NNTCF (Non-Newtonian Casson Fluid) with the inclusion of variation in enthalpy. From his work, it was reported that Casson fluid parameters, variable viscosity, suction coefficient, and curvature parameters lead to oscillatory behavior in the velocity profile. Akbar and Mohammad [10] provided a separate mathematical analysis related to the fundamental characteristics of cilia-driven transport in non-Newtonian couple stress fluid while considering electroosmosis and heat transfer effects. In another related review, Khan et al. [11] analyzed the mass and heat transmission appearances of the steady Casson fluid flow over a stretched surface immersed in a polymer medium considering the belongings of thermal radiation and internal heat generation. Verma and Mandal [12] discussed briefly the computational methods for the study of heat and mass transfer in Casson fluids. Aneja et al. [13] performed analysis of natural convection in a partially heated porous enclosure filled with Casson fluid. They found that both heat transfer and flow circulation rose with the increase in Darcy number and the Casson fluid parameter. Kumar et al. [14] conducted a detailed analysis regarding heat transfer performance owing to electrically conducting Casson fluid flow over a rotating surface under convective boundary circumstances. Several other studies also contributed to further development of the Casson fluid models [15-19].

A very important field of research is the flow of fluids over stretching surfaces, as it provides an excellent model for extrusion, wire coating, glass fiber production, and cooling of metal plates. Nonlinear stretching rates provide a better manifestation of the real situation than the usual linear stretching assumptions in most practical situations. In many such situations, the flow region is also porous and there is partial penetration of fluid through the surface, which may be of immense importance in stabilizing the flow and in the control of thermal characteristics of heat transfer. The Darcy–Forchheimer model describes such porous media, considering both viscous (Darcy) and inertial (Forchheimer) resistance effects, and hence delivers a supplementary realistic demonstration of momentum transport in high-speed regions. Reddy et al. [20] have presented a numerical study on the effects of Cattaneo–Christov heat flux in hydromagnetic flow of non-Newtonian fluids, Maxwell, Jeffrey, and Oldroyd-B models, within a Darcy–Forchheimer porous medium. The combined effects of thermal radiation, non-uniform heat sources/sinks, and variable thermal conductivity have been considered. Raza and Wang [21], on the other hand, reported heat transfer analysis in the two-dimensional Darcy–Forchheimer porous medium with magnetized nanoparticles. A very comprehensive study revealed substantial insight into the complex interaction of mechanisms that control the ternary ferrofluid flow and thermal performance in dual porosity media and hence provided a useful guide to the improvement of thermal systems based on fluids. Kumar et al. [22] proposed a mathematical model to study the heat transmission and melting flow of Reiner–Philipoff fluid over a surface inside a Darcy–Forchheimer medium.

The presence of magnetic fields, and in turn, magnetohydrodynamic (MHD) flows, is of prime importance in electrically conductive fluids that are associated with various metallurgical processes, cooling systems, and electrochemical applications [23]. An applied magnetics force offers a Lorentz force performing in contradiction of the flow, which declines the velocity and meaningfully alters the heat transmission characteristics. When such MHD effects combine with the features of permeable media and nonlinearly stretching sheets, the emerging flow features develop as a great complexity. Chamkha [24] studied the unsteady magneto-hydrodynamic (MHD) convection heat and mass transfer over a semi-infinite vertical permeable plate, taking into account the effects of heat absorption. Based on this study, Mithreya et al. [25] explored how chemical reactions affect a similar conformation. Ahmed and Agrawalla [26] discovered the unsteady MHD mass flow past a rapidly moving upright plate in the incidence of both a heat sink and a chemical reaction. Chaudhary and Ahmed [27], considering the belongings of heat sink and chemical reaction, concentrated on the power of the Soret effect in unsteady MHD convective flow over a permeable upright plate. Naramgar et al. [28] analyzed the combined effects of a inclined magnetic field, radiation, and rotation, and studied the unsteady hydromagnetic convection near a moving vertical plate in a passive medium. Manjula and Muthukumaraswami [29] studied heat and mass transfer on an infinite vertical plate under Hall current and thermal radiation, assuming a variable wall temperature. Ghosh et al. [30] investigated three-dimensional unsteady nanofluid flow over a stretching sheet, incorporating the effects of both magnetic field and radiation. Raghunath et al. [31] developed an analytical model for oscillating Casson fluid flow near an inclined vertical porous plate, including the effects of heat absorption and chemical reaction to describe the convective MHD heat and mass transfer behavior. Kumar et al. [32] analyzed the combined effect of thermal dispersion and an inclined magnetic field on such flow systems.

Besides, temperature dependence of viscosity plays an important role in accurately predicting the heat transfer performance for many non-Newtonian fluids. In most practical applications, the viscosity decreases exponentially with increase in temperature, which in turn affects the boundary layer thickness and thermal gradients. Ignoring this may give large discrepancies between the theoretical predictions and the experimental results under high temperature gradient or in the presence of thermal radiation. Pop et al. [33] presented a seminal contribution to the flow of liquids over a moving flat plate, which subsequently formed a bedrock to the investigations on drawn surfaces [34, 35] and mixed convection over vertical walls [36]. Based on such a development, thorough physical analyses were made for the flow of Newtonian fluid over a range of plate geometries [37, 38]. Recently, including

the effects of variable viscosity, magnetohydrodynamics, thermophoresis, and radiative heat transfer, a number of contributions have been made as extensions of these studies. Such advanced investigations carried out inspect the effects of combined variations in temperature-reliant viscosity and variable electrical conductivity on convective flow over inclined and permeable surfaces [39-41] for a more realistic view of a range of complex engineering and natural fluid flows.

The present study, influenced by these ideas, examines the Darcy-Forchheimer magnetohydrodynamic flow of a Casson fluid over a nonlinear porous stretching sheet, including temperature-dependent viscosity. The developed mathematical model combines the momentum and energy equations along with appropriate boundary conditions to understand the effects of nonlinearity, porosity, magnetic field strength, and viscosity variation on the flow and heat transfer characteristics. Numerical solutions are obtained through an efficient computational scheme and results presented with emphasis on dimensionless parameters characterizing combined physical effects. Based on this work, one can achieve a better understanding of nonlinear MHD flow mechanisms within porous media and find key insights for the design of advanced thermal-fluid engineering systems.

2. Mathematical formulation

We consider a nonlinear stretchable surface in a Darcy–Forchheimer porous medium assigned with an incompressible Casson fluid. The flow domain occupies the region $y > 0$, while the stretchable sheet lies along the plane $y = 0$ as described in Fig. 1. A uniform magnetic field of power B_0 is applied upright to the surface along the y-axis, giving rise to magnetohydrodynamic (MHD) effects that influence the momentum transport within the electrically conducting Casson fluid. The magnetic Reynolds number is supposed to be small enough to neglect the induced magnetic field compared to the applied one. The fluid motion is generated by the nonlinear stretching of the surface due to two identical and conflicting forces acting along the x-axis. The velocity of the stretching surface is expressed as $u_b = mx^{\eta}$, where m is a constant, η is the nonlinear stretching sheet parameter, and x is the coordinate along the stretching direction.

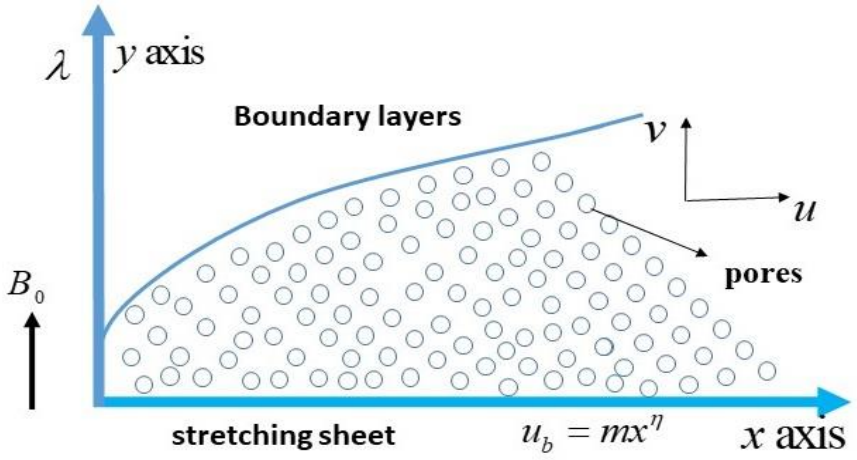

Figure 1 Design of model organism and co-ordinate arrangement.

All fluid belongings are considered constant except for the dynamic viscosity μ, which varies with temperature in accordance with the temperature-dependent behaviour of the Casson fluid. The rheological concert of a Casson liquid can be defined as [42-45] :

$$\varsigma_{ij} = \begin{cases} 2\left(\mu + \dfrac{\xi_S}{\sqrt{2\sigma}}\right)e_{ij}, & \sigma > \sigma_c, \\ 2\left(\mu + \dfrac{\xi_S}{\sqrt{2\sigma_c}}\right)e_{ij}, & \sigma < \sigma_c. \end{cases} \tag{1}$$

Here, ς_{ij} signifies the stress tensor, ξ_S and μ specify the yield stress and elastic viscosity of the Casson fluid,

respectively, e_{ij} epitomizes the deformation rate, $\sigma = e_{ij}e_{ij}$ and σ_c is the threshold assessment of σ. The yield stress of the Casson fluid ξ_S can be writeen as [46]:

$$\xi_S = \mu\frac{\sqrt{2\sigma}}{\delta}. \tag{2}$$

Here δ signifies the Casson factor. On using Eq. (2) and considering the case of flowing$\left(\eta > \eta_c\right)$, Eq. (1) becomes:

$$\varsigma_{ij} = 2\mu\left(1+\frac{1}{\delta}\right)e_{ij}. \tag{3}$$

Here for two-dimensional $e_{ij} = e_{xy} = \frac{1}{2}\left(\frac{\partial u}{\partial y}+\frac{\partial v}{\partial x}\right) = \frac{1}{2}\frac{\partial u}{\partial y}$. Then Eq. (3) becomes:

$$\varsigma_{ij} = \mu\left(1+\frac{1}{\delta}\right)\frac{\partial u}{\partial y}. \tag{4}$$

Considering the Casson fluid version of Darcy-Forchheimer law and boundary layer estimations, the continuity, momentum, and energy equations under this model are expressed as [47-49]:

$$\frac{\partial u}{\partial x}+\frac{\partial v}{\partial y} = 0, \tag{5}$$

$$u\frac{\partial u}{\partial x}+v\frac{\partial u}{\partial y} = \frac{1}{\rho}\frac{\partial}{\partial y}\left[\mu(\theta)\left(1+\frac{1}{\delta}\right)\frac{\partial u}{\partial y}\right]-\frac{\mu(\theta)}{\rho K}\left(1+\frac{1}{\delta}\right)u - Fu^2 - \frac{sB_0^2}{\rho}u, \tag{6}$$

$$u\frac{\partial \theta}{\partial x}+v\frac{\partial \theta}{\partial y} = \alpha\frac{\partial^2\theta}{\partial y^2}. \tag{7}$$

Exposed to the boundary circumstances as:

$$\begin{aligned} &u = u_b = mx^{\eta},\ v = 0,\ \ \theta = \theta_b \quad \text{at}\ \ y = 0,\\ &u = v = 0,\ \theta = \theta_\infty \qquad\qquad\ \ \text{as}\ \ y\to\infty. \end{aligned} \tag{8}$$

Here, u and u display the velocities along x and y-axes, individually, ρ means the density, K means the permeability of the permeable medium, s denotes the electrical conductivity of the Casson fluid, F signifies the nonuniform inertial coefficient, u_b displays the stretching velocity, θ represents the temperature, θ_b designates the wall temperature and θ_∞ indicates the ambient temperature of the fluid. Here, μ is the temperature dependent elastic viscosity of the Casson fluid and considered as [41, 50, 51]:

$$\mu = \frac{\mu_\infty}{\left[1+\beta\left(\theta-\theta_\infty\right)\right]}. \tag{9}$$

Here, μ_∞ denotes the ambient viscosity of the Casson fluid and β is constant. On using Eq. (9) in Eq. (6), we have:

$$\begin{aligned} u\frac{\partial u}{\partial x}+v\frac{\partial u}{\partial y} = {} & \frac{\mu_\infty}{\rho\left[1+\beta\left(\theta-\theta_\infty\right)\right]}\left(1+\frac{1}{\delta}\right)\left[-\frac{\beta}{\left[1+\beta\left(\theta-\theta_\infty\right)\right]}\frac{\partial\theta}{\partial y}\frac{\partial u}{\partial y}+\frac{\partial^2 u}{\partial y^2}-\frac{u}{K}\right]\\ & - Fu^2 - \frac{sB_0^2}{\rho}u. \end{aligned} \tag{10}$$

Now introduce the following similarity transformations [52, 53]:

$$\lambda = y\sqrt{\frac{m(\eta+1)}{2\upsilon_\infty}}x^{\frac{\eta-1}{2}},\ u = mx^{\eta}g'(\lambda),\ \ \Theta(\lambda) = \frac{\theta-\theta_\infty}{\theta_b-\theta_\infty},$$
$$v = -\sqrt{\frac{m\upsilon_\infty(\eta+1)}{2}}x^{\frac{\eta-1}{2}}\left[g(\lambda)+\left(\frac{\eta-1}{\eta+1}\right)\lambda g'(\lambda)\right]. \tag{11}$$

Here, $\upsilon_\infty = \frac{\mu_\infty}{\rho}$ is the kinetic viscosity of the Casson fluid and η is the nonlinear factor of the stretching sheet. On using Eq. (11), Eq. (10) and Eq. (7) become:

$$\left(1+\frac{1}{\delta}\right)(1+Q\Theta)g''' - \frac{2\eta}{(\eta+1)}\left[(1+Q\Theta)g'\right]^2 + (1+Q\Theta)^2 gg'' - \left(1+\frac{1}{\delta}\right)Qg''\Theta'$$
$$-\left(1+\frac{1}{\delta}\right)\frac{2(1+Q\Theta)\varepsilon g'}{(\eta+1)} - \frac{2M}{(\eta+1)}(1+Q\Theta)^2 g' - \frac{2F_r}{(\eta+1)}\left[(1+Q\Theta)g'\right]^2 = 0, \tag{12}$$

$$\Theta'' + P_r g\Theta' = 0. \tag{13}$$

The boundary conditions Eq. (4) reduces as:

$$\begin{aligned} &g = 0,\ g' = 1,\ \Theta = 1 \ \text{ at } \ \lambda = 0,\\ &g' = 0,\ \ \Theta = 0 \qquad\quad \text{as } \ \lambda \to \infty. \end{aligned} \tag{14}$$

Here $(\ )'$ means the derivative with respect to λ, $Q = \beta(\theta_b - \theta_\infty)$ denotes the viscosity variation parameter, $\varepsilon = \frac{\upsilon_\infty}{Kmx^{n-1}}$ denotes the porosity parameter, $P_r = \frac{\upsilon_\infty}{\alpha}$ symbolizes the Prandtl number, $M = \frac{2sB_0^2}{\rho m x^{\eta-1}}$ denotes the magnetic parameter and $F_r = Fx$ symbolizes the Forchheimer number. The skin friction and heat spread rate are represented by respectively, $f''(0)$ and $-\theta'(0)$.

3. Numerical Practice

The analytical resolution of Eqs. (12) and (13) under the edge circumstances specified in Eq. (14) is not feasible due to the pronounced nonlinearity and interdependence of the equations. Therefore, a numerical tactic employing the shooting method in combination with the bvp5c solver is adopted. Before arranged with the computation, the prevailing equations are reformulated into a scheme of first-order ordinary differential equations. To achieve this, we define:

$$g = r_1, g' = r_2,\ g'' = r_3,\ g''' = r_3',\ \Theta = r_4,\ \Theta' = r_5,\ \Theta'' = r_5'. \tag{15}$$

Thus Eq. (12), Eq. (13) and Eq. (14) are become as:

$$r_1' = r_2, \tag{16}$$

$$r_2' = r_3, \tag{17}$$

$$r_3' = -\frac{1}{\left(1+\frac{1}{\delta}\right)(1+Qr_4)}\left[-\frac{2\eta}{(\eta+1)}\left[(1+Qr_4)r_2\right]^2 + (1+Qr_4)^2 r_1 r_3 - \left(1+\frac{1}{\delta}\right)Qr_3 r_5\right.$$
$$\left.-\left(1+\frac{1}{\delta}\right)\frac{2(1+Qr_4)\varepsilon r_2}{(\eta+1)} - \frac{2M}{(\eta+1)}(1+Qr_4)^2 r_2 - \frac{2F_r}{(\eta+1)}\left[(1+Qr_4)r_2\right]^2\right], \tag{18}$$

$$r_4' = r_5, \tag{19}$$

$$r_5' = -P_r r_1 r_5, \tag{20}$$

$$r_1(0) = 0,\ \ r_2(0) = 1,\ r_4(0) = 1,\ r_2(\infty) = 0,\ r_4(\infty) = 0. \tag{21}$$

In the shooting algorithm, the computation starts with assumed values for the unknown boundary conditions at

$\lambda = 0$ and $\lambda \to \infty$. These initial estimations are then systematically distinguished through iterative alterations till the numerical outcomes converge to a stable solution. To accomplish a high level of numerical precision, the Runge–Kutta technique with results also confirmed by MATLAB's bvp5c solver is designed with relative and absolute tolerances of 10^{-3} and 10^{-4}, respectively. Once convergence is reached, the resulting velocity and temperature fields are analysed, and corresponding values of skin friction and heat transfer rate are determined. The influence of the controlling parameters ε, M, P_r, δ, Q, F_r and η is examined by altering one parameter at a time while keeping others constant as $\varepsilon = 0.6$, $M = 5$, $P_r = 2$, $Q = 0.6$, $\eta = 2$, $\delta = 0.6$ and $F_r = 1.5$. The selected parameter ranges are consistent with those commonly found in previously published literature [7, 54-63] .

Table 1 Contrast of Skin friction $g''(0)$ for numerous standards of $M' = \dfrac{2M}{(\eta+1)}$ and $a = \dfrac{2\eta}{(\eta+1)}$ at $Q = \varepsilon = P_r = F_r = 0$ and $\delta \to \infty$.

M'	$a=1$			$a=5$	
	Present Study	Ganji et al. [64]	Hayat et al. [65]	Present Study	Hayat et al. [65]
0	-1.00048	-1.00000	-1.00000	-1.90262	-1.9098
1	-1.41422	-1.41349	-1.41412	-2.15286	-2.1528
5	-2.44949	-2.44019	-2.44948	-2.94144	-2.9414
10	-3.31662	-3.31636	-3.31662	-3.69567	-3.6956
50	-7.14143	-7.14098	-7.14142	-7.32568	-7.3256
100	-10.0499	-10.04926	-10.04987	-10.18180	-10.1816
500	- 22.3830	-22.38147	-22.38302	-22.44264	-22.4425
1000	-31.6386	-31.63672	-31.63858	-31.68072	-31.6806

Table 2 Contrast of Skin friction $g''(0)$ for numerous values of δ at $Q = \varepsilon = P_r = F_r = M = 0$ and $\eta = 1$.

δ	Present Study	Nandeppanavar [66]
0.5	-0.581988	-0.57735
1.0	-0.709388	-0.707107
1.5	-0.776187	-0.774597
2.0	-0.817769	-0.816497
2.5	-0.846248	-0.845154
3.0	-0.867005	-0.866025

Table 3 Contrast of heat spread rate $-\Theta'(0)$ for numerous values of P_r and η at $Q = \varepsilon = F_r = M = 0$ and $\delta \to \infty$.

P_r	$\eta=1$		$\eta=10$	
	Present Study	Alessa et al. [54]	Present Study	Cortell [67]
1	0.583865		0.557831	0.554960
2	0.911092	0.911358		
3	1.165018			
5	1.567870		1.528773	1.528573
7	1.895238	1.895407		

Table 4 Comparison of heat spread rate $-\Theta'(0)$ and Skin friction $g''(0)$ for numerous values of η, δ, Q and M at $P_r = 2$, $F_r = 1.5$ and $\varepsilon = 0.6$.

η	δ	Q	$M=0$		$M=5$		$M=10$	
			$-\Theta'(0)$	$g''(0)$	$-\Theta'(0)$	$g''(0)$	$-\Theta'(0)$	$g''(0)$
1	0.5	0	0.8946382	-1.123614	0.7711454	-1.712209	0.6916693	-2.144518
		0.3	0.8727622	-1.271855	0.7363051	-1.953004	0.6519475	-2.448592
		0.6	0.8543142	-1.393651	0.7069739	-2.156846	0.6193816	-2.709047
		0.9	0.8383852	-1.497522	0.6817016	-2.336029	0.5920208	-2.940406
	1.0	0	0.8696362	-1.261827	0.7157422	-2.024177	0.6272072	-2.568728
		0.3	0.8455472	-1.431782	0.6774677	-2.310535	0.5861216	-2.933355
		0.6	0.8251622	-1.573047	0.6457537	-2.555228	0.5533521	-3.248332
		0.9	0.8074822	-1.694962	0.6188478	-2.772118	0.5264804	-3.529947
	1.5	0	0.8561622	-1.337843	0.6884121	-2.190129	0.5973398	-2.792491
		0.3	0.8309352	-1.519522	0.6489609	-2.500393	0.5563587	-3.188833
		0.6	0.8095622	-1.671297	0.6165976	-2.766574	0.5241217	-3.532387
		0.9	0.7910032	-1.802936	0.5893954	-3.003287	0.4979902	-3.840306
	10^9	0	0.8101895	-1.606065	0.6068254	-2.755745	0.5148858	-3.549166
		0.3	0.7813941	-1.828199	0.5660924	-3.146574	0.4765922	-4.052251
		0.6	0.7569996	-2.016251	0.5338332	-3.485294	0.4476143	-4.491926
		0.9	0.7360656	-2.181567	0.5075362	-3.788822	0.4248285	-4.888098
3	0.5	0	0.9306784	-0.952093	0.8504899	-1.319858	0.7912061	-1.605051
		0.3	0.9093610	-1.098805	0.8197808	-1.523944	0.7549946	-1.850386
		0.6	0.8909824	-1.221549	0.7933385	-1.696011	0.7242393	-2.058368
		0.9	0.8748395	-1.327322	0.7701364	-1.845956	0.6976106	-2.240962
	1.0	0	0.9029273	-1.099096	0.8019319	-1.569326	0.7318709	-1.927221
		0.3	0.8792075	-1.267682	0.7671698	-1.808878	0.6920286	-2.217335
		0.6	0.8587742	-1.409446	0.7375077	-2.012035	0.6588422	-2.465033
		0.9	0.8408101	-1.532455	0.7117073	-2.190376	0.6306279	-2.684138
	1.5	0	0.8881985	-1.178491	0.7771982	-1.701538	0.7028371	-2.096896
		0.3	0.8632612	-1.358681	0.7406615	-1.959612	0.6617804	-2.410408
		0.6	0.8417867	-1.510584	0.7096872	-2.179126	0.6279728	-2.679003
		0.9	0.8229019	-1.642807	0.6829157	-2.372472	0.5995273	-2.917356
	10^9	0	0.8386987	-1.453212	0.6995042	-2.150581	0.6168872	-2.669858
		0.3	0.8099283	-1.672793	0.6589816	-2.470843	0.5746435	-3.062117
		0.6	0.7852206	-1.859301	0.6255621	-2.745757	0.5411723	-3.401418
		0.9	0.7637823	-2.023253	0.5974053	-2.990069	0.5139162	-3.704902

3.1. Validation

To ascertain the reliability and exactitude of the numerical approach employed in this analysis, preliminary validation simulations were performed. In these tests, the effects of viscosity variation, the Prandtl number, the Forchheimer number, and the influence of the porous medium were neglected, thereby representing the flow of a Newtonian fluid in a regular medium. Simulations were carried out for a range of values of the modified magnetic field factor $\left(M' = \frac{2M}{(\eta+1)} \right)$ and the modified nonlinear stretching factor $\left(a = \frac{2\eta}{(\eta+1)} \right)$. The resulting data were benchmarked against the findings of Ganji et al. [64] and Hayat et al. [65], as presented in Table 1. Table 2 offerings a comparison with the results of Nandeppanavar [66], in which the skin friction coefficient $g''(0)$ was evaluated for various values of the Casson factor δ under the conditions of $Q = \varepsilon = P_r = F_r = M = 0$ and $\eta = 1$.

Furthermore, Table 3 provides a comparative analysis with the studies of Alessa et al. [54], Rana and Bhargava [55] and Cortell [67], for diverse Prandtl numbers P_r and nonlinear stretching factors η, under the limiting assumptions of this investigation, namely, neglecting viscosity variation factor, the Forchheimer number and magnetic field effect, and considering a Newtonian fluid in a regular medium. The excellent agreement obtained in all comparisons attests to the robustness, accuracy, and credibility of the numerical approach adopted in this work.

Table 5 Comparison of heat spread rate $-\Theta'(0)$ and Skin friction $g''(0)$ for various values of η, Q, δ and ε at $P_r = 2$, $F_r = 1.5$ and $M = 10$.

η	δ	Q	$\varepsilon = 0$		$\varepsilon = 0.5$		$\varepsilon = 1.0$	
			$-\Theta'(0)$	$g''(0)$	$-\Theta'(0)$	$g''(0)$	$-\Theta'(0)$	$g''(0)$
1	0.5	0	0.7170127	-1.999698	0.6956823	-2.121069	0.6763742	-2.235854
		0.3	0.6738503	-2.317545	0.6554138	-2.427304	0.6387383	-2.531757
		0.6	0.6382468	-2.589321	0.6223715	-2.689533	0.6079707	-2.785504
		0.9	0.6083164	-2.829855	0.5946098	-2.922335	0.5821171	-3.011391
	1.0	0	0.6450124	-2.44912	0.6300552	-2.549184	0.6162547	-2.64546
		0.3	0.6007588	-2.826086	0.5884657	-2.915777	0.5770945	-3.002549
		0.6	0.5654565	-3.150718	0.5552955	-3.232294	0.5458505	-3.311597
		0.9	0.5365968	-3.439974	0.5281093	-3.515136	0.5201758	-3.588489
	1.5	0	0.6122132	-2.682877	0.5997287	-2.774523	0.5881172	-2.863234
		0.3	0.5683076	-3.090838	0.5582815	-3.172728	0.5489217	-3.252394
		0.6	0.5338302	-3.443333	0.5256883	-3.51772	0.5180468	-3.59039
		0.9	0.5059948	-3.758268	0.4992855	-3.826771	0.4929534	-3.893915
	10^9	0	0.5232795	-3.463582	0.5162483	-3.535046	0.5095732	-3.605092
		0.3	0.4829372	-3.976241	0.4776232	-4.039687	0.4725511	-4.102122
		0.6	0.4525531	-4.423039	0.4484205	-4.480524	0.4444546	-4.537227
		0.9	0.4287749	-4.824715	0.4254742	-4.877596	0.4222917	-4.929863
3	0.5	0	0.8108573	-1.508632	0.7943678	-1.589388	0.7789762	-1.666226
		0.3	0.7731637	-1.761592	0.7579108	-1.835943	0.7437373	-1.906872
		0.6	0.7408286	-1.976624	0.7268993	-2.045043	0.7139793	-2.110582
		0.9	0.7126722	-2.165298	0.7000256	-2.228598	0.6882935	-2.289499
	1.0	0	0.7468009	-1.847686	0.7342894	-1.914195	0.7224588	-1.978463
		0.3	0.7052723	-2.145083	0.6941714	-2.205483	0.6836982	-2.264031
		0.6	0.6704897	-2.398975	0.6607267	-2.454177	0.6515136	-2.507882
		0.9	0.6408582	-2.623182	0.6322846	-2.674103	0.6241803	-2.723809
	1.5	0	0.7158042	-2.024039	0.7049431	-2.084931	0.6946219	-2.144088
		0.3	0.6730398	-2.344554	0.6636078	-2.399576	0.6546556	-2.453197
		0.6	0.6376948	-2.61893	0.6295515	-2.669105	0.6218146	-2.718163
		0.9	0.6079339	-2.861972	0.6008939	-2.908217	0.5941905	-2.953564
	10^9	0	0.6250622	-2.613024	0.6182232	-2.660472	0.6116449	-2.707082
		0.3	0.5812953	-3.011295	0.5757314	-3.053711	0.5703715	-3.095491
		0.6	0.5466245	-3.355259	0.5420651	-3.393774	0.5376622	-3.431798
		0.9	0.5184382	-3.662413	0.5146577	-3.69786	0.5109972	-3.732918

4. Result and Discussion

Fig. 2 and Fig. 3 depict the variations in velocity and temperature profiles for different values of the Prandtl number P_r and the nonlinear factor of the stretching sheet η. The results indicate that an increase in both the Prandtl number P_r and the nonlinear factor of the stretching sheet η leads to an enhancement in the velocity profile and a

reduction in the temperature profile. The influence of the Prandtl number P_r arises from the fact that higher values correspond to lower thermal diffusivity comparative to momentum diffusivity, resulting in slower heat diffusion compared to momentum transfer. Subsequently, the velocity boundary layer converts thicker, whereas the thermal boundary layer develops thinner, creating higher velocity and lesser temperature allocations near the wall. Similarly, the consequence of the nonlinear factor of the stretching sheet η can be ascribed to the strengthened stretching of the sheet, which augments fluid motion at the surface, endorses momentum exchange, and hurries heat transmission. This increased stretching consequently eases the thickness of the thermal boundary layer.

Table 6 Comparison of heat spread rate $-\Theta'(0)$ and Skin friction $g''(0)$ for various values of η, Q, δ and ε at $P_r = 2$, $\varepsilon = 0.6$ and $M = 10$.

η	δ	Q	$F_r = 0$		$F_r = 0.5$		$F_r = 1.0$	
			$-\Theta'(0)$	$g''(0)$	$-\Theta'(0)$	$g''(0)$	$-\Theta'(0)$	$g''(0)$
1	0.5	0	0.6995582	-2.065591	0.6968759	-2.092228	0.6942469	-2.118533
		0.3	0.6599018	-2.358328	0.6571952	-2.388793	0.6545443	-2.418876
		0.6	0.6273095	-2.608519	0.6246094	-2.642451	0.6219676	-2.675955
		0.9	0.5998674	-2.830389	0.5971932	-2.867528	0.5945783	-2.904194
	1.0	0	0.6353076	-2.469818	0.6325472	-2.503218	0.6298477	-2.536183
		0.3	0.5940544	-2.820377	0.5913485	-2.858529	0.5887051	-2.896182
		0.6	0.5610592	-3.122635	0.5584282	-3.165084	0.5558599	-3.206976
		0.9	0.5339397	-3.392537	0.5313915	-3.438946	0.5289062	-3.484742
	1.5	0	0.6053786	-2.683282	0.6026364	-2.720167	0.5999577	-2.756564
		0.3	0.5641221	-3.064139	0.5614714	-3.106256	0.5588845	-3.147813
		0.6	0.5315775	-3.393708	0.5290299	-3.440551	0.5265456	-3.486769
		0.9	0.5051378	-3.688766	0.5026942	-3.739956	0.5003124	-3.790461
	10^9	0	0.5222804	-3.405877	0.5197518	-3.454294	0.5172882	-3.502048
		0.3	0.4834667	-3.888754	0.4811136	-3.944215	0.4788223	-3.998489
		0.6	0.4540288	-4.310245	0.4518329	-4.371638	0.4496957	-4.432187
		0.9	0.4308381	-4.689755	0.4287803	-4.756781	0.4267782	-4.822883
3	0.5	0	0.7978276	-1.552561	0.7955855	-1.570249	0.7933787	-1.587744
		0.3	0.7618586	-1.790642	0.7595333	-1.810775	0.7572457	-1.830687
		0.6	0.7312563	-1.992133	0.7288781	-2.014453	0.7265396	-2.036528
		0.9	0.7047213	-2.168724	0.7023101	-2.193066	0.6999404	-2.217142
	1.0	0	0.7390866	-1.861618	0.7366392	-1.883735	0.7342344	-1.905625
		0.3	0.6993517	-2.142718	0.6968663	-2.167874	0.6944258	-2.192743
		0.6	0.6661795	-2.382302	0.6636878	-2.410193	0.6612425	-2.437766
		0.9	0.6379232	-2.593906	0.6354442	-2.624325	0.6330131	-2.654399
	1.5	0	0.7102142	-2.024531	0.7077122	-2.048932	0.7052515	-2.073052
		0.3	0.6691812	-2.328107	0.6666674	-2.355857	0.6642012	-2.383287
		0.6	0.6353145	-2.587742	0.6328161	-2.618513	0.6303712	-2.648929
		0.9	0.6067521	-2.817822	0.6042952	-2.851381	0.6018873	-2.884556
	10^9	0	0.6242779	-2.575101	0.6217637	-2.607063	0.6193008	-2.638644
		0.3	0.5817874	-2.954322	0.5793553	-2.990679	0.5769746	-3.026606
		0.6	0.5480334	-3.281852	0.5456961	-3.322182	0.5434097	-3.362029
		0.9	0.5204932	-3.574505	0.5182516	-3.618486	0.5160599	-3.661946

Fig. 4 and Fig. 5 illuminates the outcome of the porosity factor ε and the Forchheimer number F_r on the velocity and temperature profiles. It is marked from these figures that accumulative both the porosity factor ε and the Forchheimer number F_r leads to a decline in the velocity profile and a rise in the temperature profile. Physically,

a greater porosity factor suggests that the permeable medium exerts bigger confrontation to fluid motion, thereby sinking the velocity within the boundary layer. This decline in velocity drops the rate of heat dissipation from the surface and declines convective conveyance, causing an increase of thermal energy within the boundary layer and an associated upsurge in temperature. The power of the Forchheimer number F_r reveals a similar trend. A larger Forchheimer number characterizes stronger inertial resistance within the permeable medium, which further delays fluid motion and suppresses flow velocity. The reduced fluid movement reduces convective heat allocation efficiency, prominent to fewer effective cooling of the boundary layer. As a result, the velocity declines, while the temperature profile surges due to the build-up of thermal energy near the surface.

Table 7 Comparison of heat spread rate $-\Theta'(0)$ and Skin friction $g''(0)$ for various values of η, Q, δ and ε at $F_r = 1.5$, $\varepsilon = 0.6$ and $M = 10$.

η	δ	Q	$P_r = 1$		$P_r = 3$		$P_r = 6$	
			$-\Theta'(0)$	$g''(0)$	$-\Theta'(0)$	$g''(0)$	$-\Theta'(0)$	$g''(0)$
1	0.5	0	0.4192888	-2.144518	0.9313101	-2.144518	1.4949751	-2.144518
		0.3	0.3956789	-2.432827	0.8844716	-2.46257	1.4398608	-2.493824
		0.6	0.3773542	-2.683938	0.8449101	-2.732546	1.3925607	-2.788432
		0.9	0.3626026	-2.909831	0.8108024	-2.970193	1.3506599	-3.044549
	1.0	0	0.3819162	-2.568728	0.8549273	-2.568728	1.4080863	-2.568727
		0.3	0.3596588	-2.919749	0.8037211	-2.946281	1.3449621	-2.977172
		0.6	0.3427986	-3.227215	0.7613531	-3.269373	1.2915289	-3.322935
		0.9	0.3294848	-3.504709	0.7255286	-3.555969	1.2444166	-3.625400
	1.5	0	0.3658031	-2.792491	0.8178089	-2.792491	1.3636982	-2.792491
		0.3	0.3444451	-3.176218	0.7652412	-3.201172	1.2974549	-3.231719
		0.6	0.3284318	-3.513013	0.7222674	-3.552188	1.2408707	-3.604232
		0.9	0.3158839	-3.817315	0.6863229	-3.864533	1.1916157	-3.931192
	10^9	0	0.3243833	-3.549166	0.7089475	-3.549166	1.2229982	-3.549166
		0.3	0.3061274	-4.042311	0.6555351	-4.062662	1.1479824	-4.091005
		0.6	0.2927732	-4.477027	0.6135742	-4.508029	1.0853196	-4.554334
		0.9	0.2824896	-4.870691	0.5796367	-4.907287	1.0319233	-4.964699
3	0.5	0	0.4861484	-1.605051	1.0407377	-1.605051	1.6111547	-1.605051
		0.3	0.4606352	-1.833294	1.0008509	-1.863844	1.5664324	-1.891193
		0.6	0.4401103	-2.029581	0.9663197	-2.082401	1.5272122	-2.134099
		0.9	0.4231362	-2.204425	0.9359113	-2.272916	1.4921454	-2.345055
	1.0	0	0.4449293	-1.927221	0.9763629	-1.927221	1.5432652	-1.927220
		0.3	0.4194652	-2.201622	0.9310017	-2.230643	1.4914218	-2.259280
		0.6	0.3995065	-2.439418	0.8921681	-2.488009	1.4465989	-2.540589
		0.9	0.3833446	-2.652433	0.8583389	-2.713848	1.4065694	-2.785304
	1.5	0	0.4263441	-2.096896	0.9437661	-2.096896	1.5079423	-2.096896
		0.3	0.4013116	-2.395451	0.8960294	-2.423512	1.4525687	-2.452514
		0.6	0.3819235	-2.654963	0.8554685	-2.701267	1.4050916	-2.753777
		0.9	0.3663726	-2.887913	0.8203906	-2.945787	1.3626912	-3.016253
	10^9	0	0.3763668	-2.669858	0.8419675	-2.669858	1.3919396	-2.669858
		0.3	0.3536864	-3.049572	0.7889665	-3.074158	1.3271028	-3.103389
		0.6	0.3366671	-3.381966	0.7452877	-3.420985	1.2712263	-3.471481
		0.9	0.3233383	-3.681675	0.7085529	-3.729059	1.2223338	-3.794406

The power of the Casson factor δ on the velocity and temperature profiles are accessible in Fig. 6. From this figures, it is witnessed that enhancing the Casson factor δ leads to a decline in the velocity profile and an upturn in the temperature profile. Physically, a larger Casson factor δ tallies to a lower stress tensor, implication the fluid

offers fewer resistance to deformation and behaves more like a Newtonian fluid. This decline in inner resistance overpowers momentum transmission near the wall, declining the velocity within the boundary layer. At the same time, the weakened convective conveyance decreases heat removal from the surface, causing thermal energy to accumulate and resulting in greater temperature profiles.

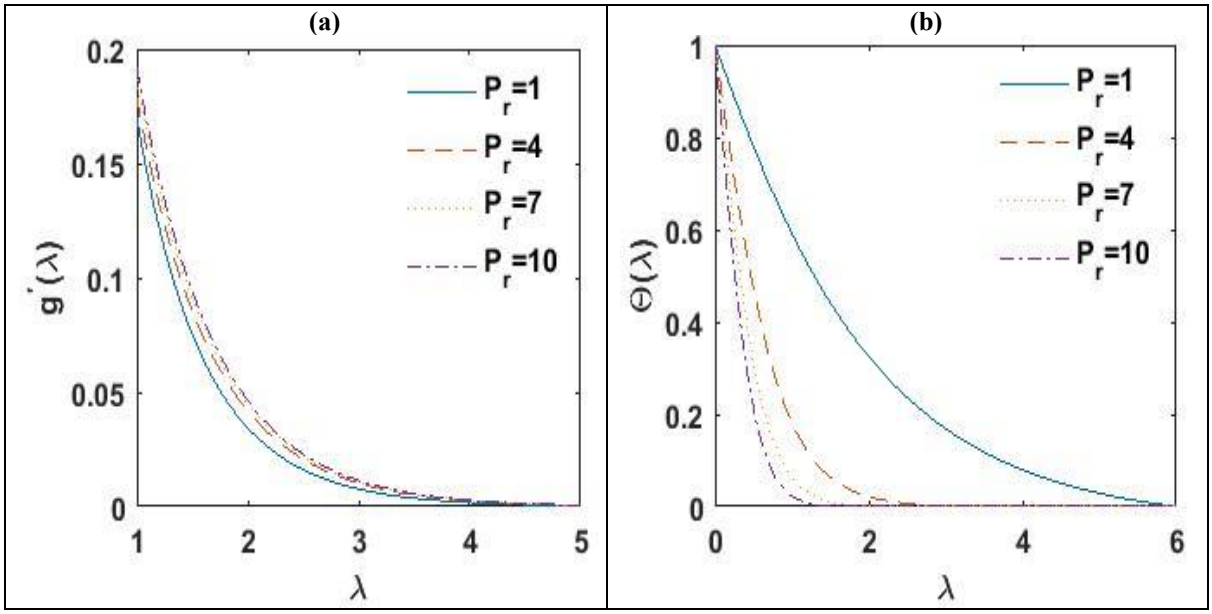

Figure 2. Impression of P_r on the (a) velocity and (b) temperature profiles.

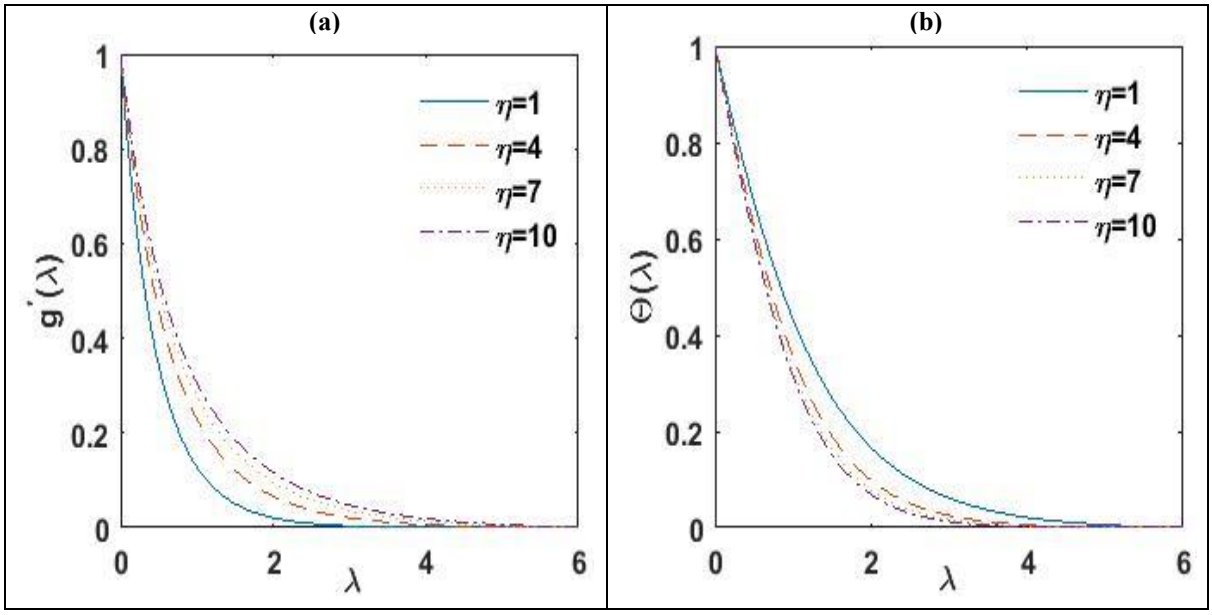

Figure 3. Impression of η on the (a) velocity and (b) temperature profiles.

Fig. 7 displays the consequence of the magnetic field factor M on the velocity and temperature profiles. It is perceived that increasing the magnetic field factor M leads to a reduction in the velocity profile and a corresponding increase in the temperature profile. This behaviour can be attributed to the Lorentz force generated by the applied magnetic field M, which acts opposite to the direction of fluid motion. The incidence of this resistive

force suppresses the fluid velocity and rises the thickness of the momentum boundary layer. As the flow slows down, convective heat conveyance is reduced, leading to the build-up of thermal energy within the boundary layer and, subsequently, greater temperature profiles.

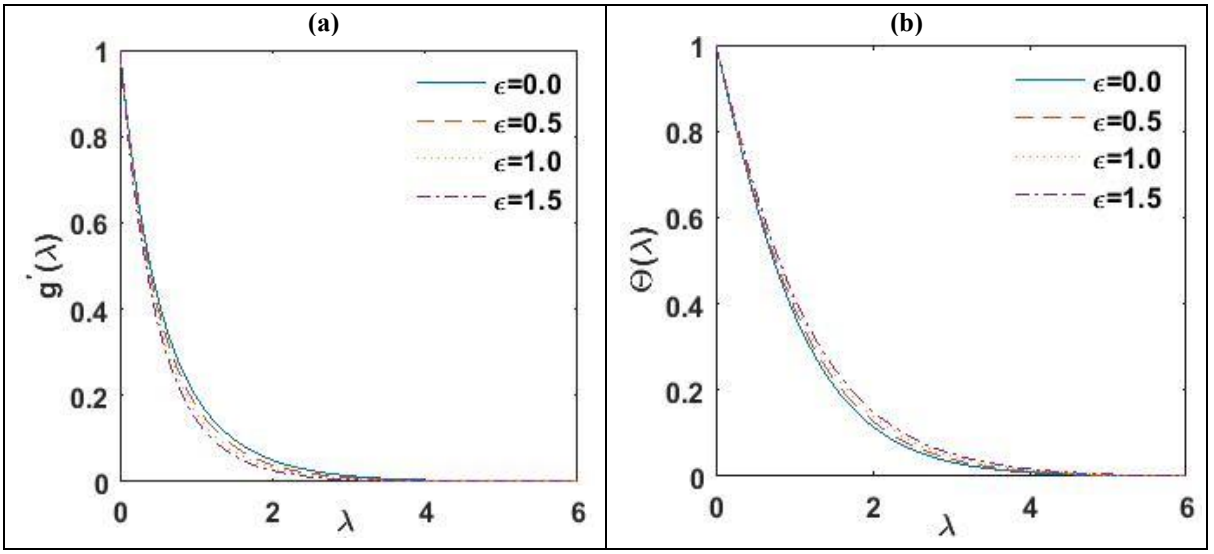

Figure 4. Impression of ε on the (a) velocity and (b) temperature profiles.

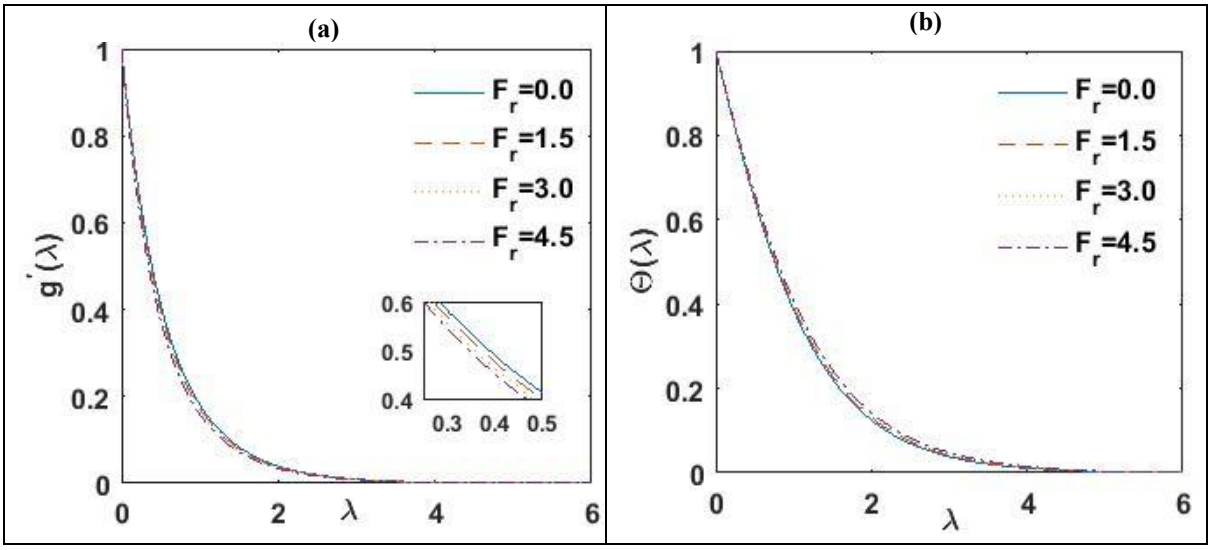

Figure 5. Influence of F_r on the (a) velocity and (b) temperature profiles.

The relationship amid the viscosity variation factor Q and the velocity and temperature shapes is offered in Fig. 8. The figure displays that elevating the viscosity variation factor Q results in a decline in the velocity profile and a simultaneous surge in the temperature profile. This effect is due to the fact that increasing the viscosity variation factor Q lowers the effective viscosity of the fluid at the surface. The reduction in viscosity limits momentum transfer, thereby reducing the velocity within the boundary layer, while simultaneously enhancing heat diffusion. As a result, the thermal energy accumulates more effectively, leading to higher temperature profiles in the flow field.

Fig. 9 depicts the changes in the heat spread rate and skin friction as influenced by the Casson factor δ with various values of the magnetic field factor M . The results are also presented in Table 4. It is evident that both the

heat spread rate and skin friction decrease with a surge in the Casson factor δ and the magnetic field factor M. Physically, an escalation in the Casson factor δ relates to a lessening in the stress, ensuing in lesser resistance to fluid motion. This lessens the velocity gradient nearby the wall, prominent to a diminution in the skin friction coefficient. The weakened velocity gradient also weakens convective heat transmission, causing a lessening in the heat transmission rate. The impact of the magnetic field factor M arises from the Lorentz force, which opposes the fluid gesture. The magnetic resistance further suppresses velocity nearby the wall, thickening the momentum boundary layer and dropping convective heat transportation, thereby sinking both the skin friction and the heat transfer rate.

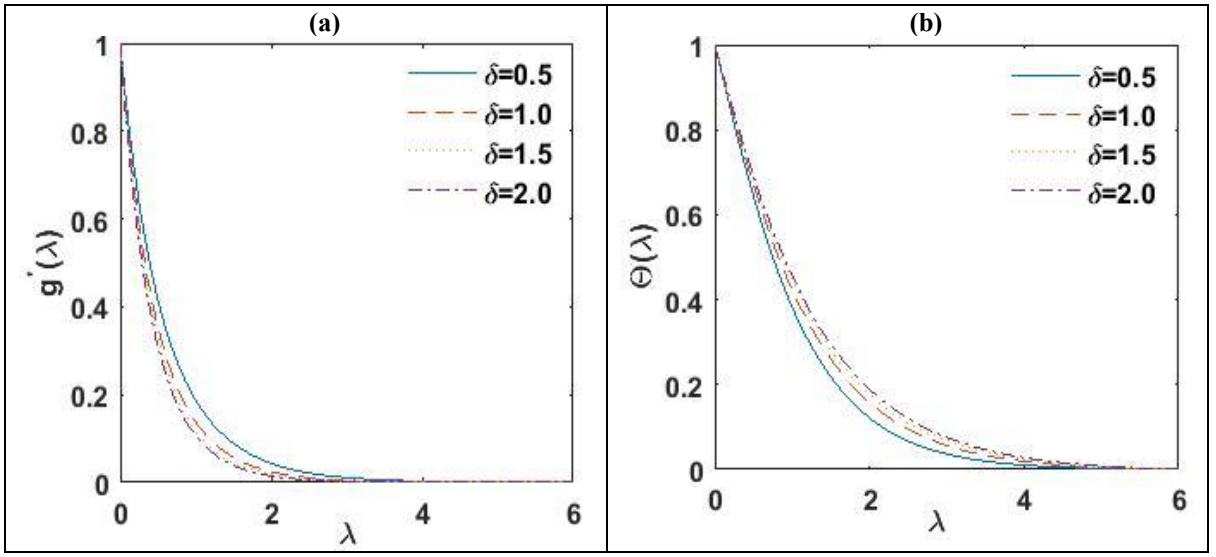

Figure 6. Impression of δ on the (a) velocity and (b) temperature profiles.

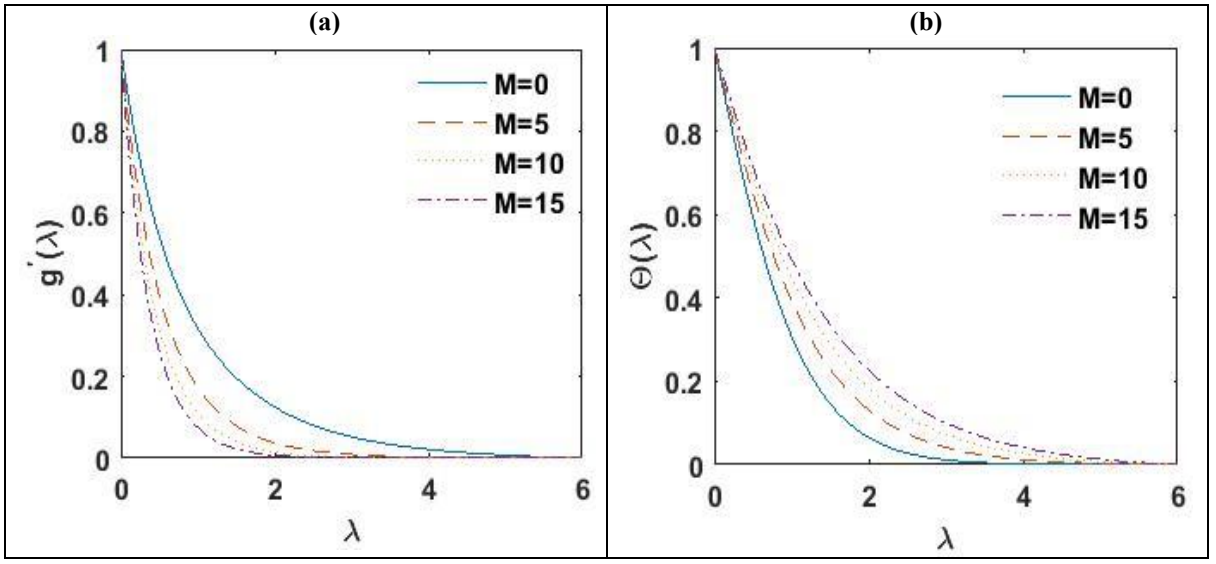

Figure 7. Impact of M on the (a) velocity and (b) temperature profiles.

Fig. 10 spectacles the outcome of the nonlinear factor of the stretching sheet η on the heat spread rate and skin friction. It is evident that both the heat spread rate and skin friction increase with a surge in the nonlinear factor of the stretching sheet η. Increasing the nonlinear stretching factor enhances the surface velocity, ensuing in higher skin friction and a thinner thermal boundary layer. This gives a sharper temperature gradient at the wall and an

increased heat transmission rate, explaining the observed deviations in velocity and temperature profiles.

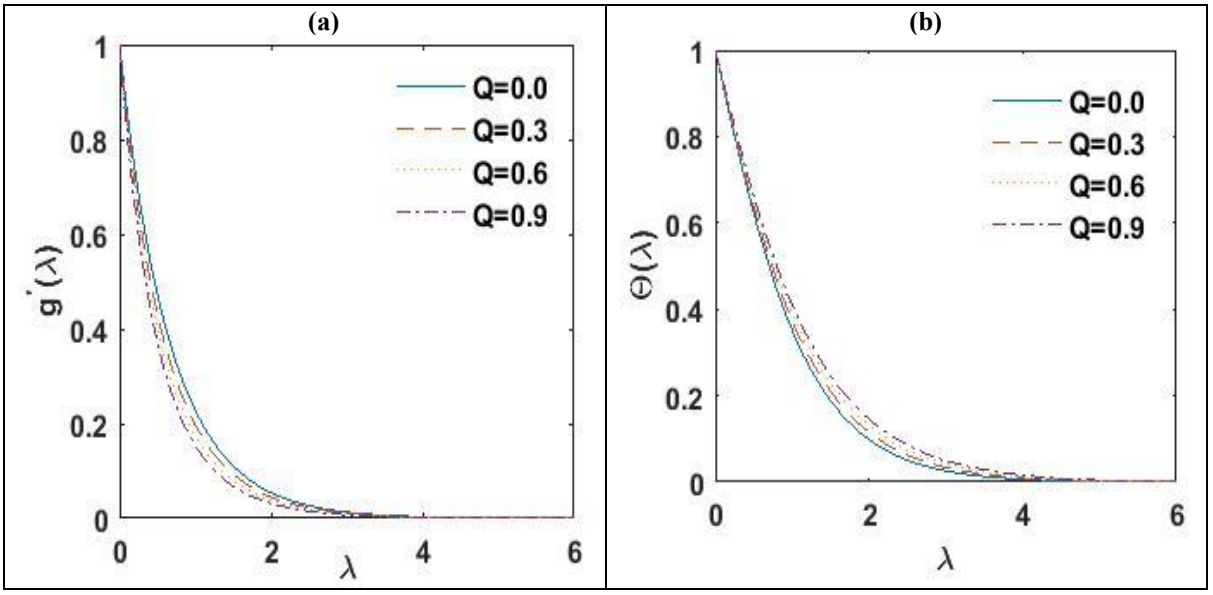

Figure 8. Impact of Q on the (a) velocity and (b) temperature profiles.

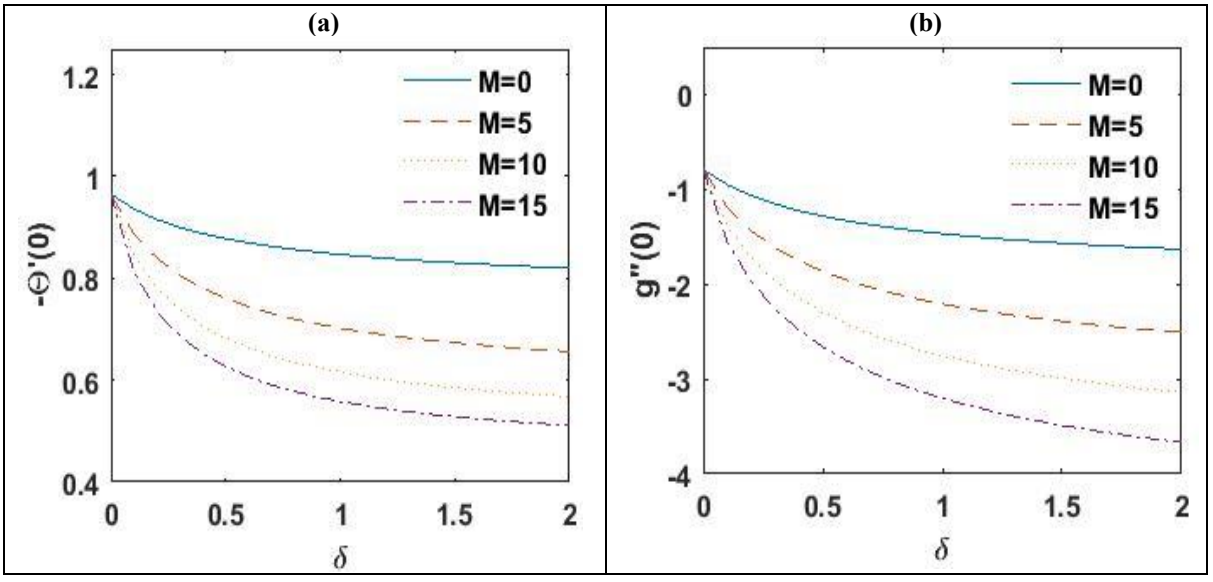

Figure 9. Impression of M on the (a) heat transfer rate and (b) skin friction.

Fig 11 and Fig. 12 respectively display the influence of the porosity parameter ε and the Forchheimer number F_r on the heat transmission rate and skin friction. The results are also recorded in Table 5 and Table 6. From these, it is found that the heat transmission rate and the skin friction decrease on growing both the porosity parameter ε and the Forchheimer number F_r . This behaviour occurs because higher porosity and larger Forchheimer numbers increase the resistance of the porous medium, slowing down the fluid within the boundary layer. The reduced velocity lowers the shear stress at the wall, resulting in decreased skin friction. At the same time, the weaker fluid motion diminishes convective heat transfer, causing the thermal boundary layer to thicken and the temperature gradient at the wall to decrease, which ultimately reduces the heat transfer rate.

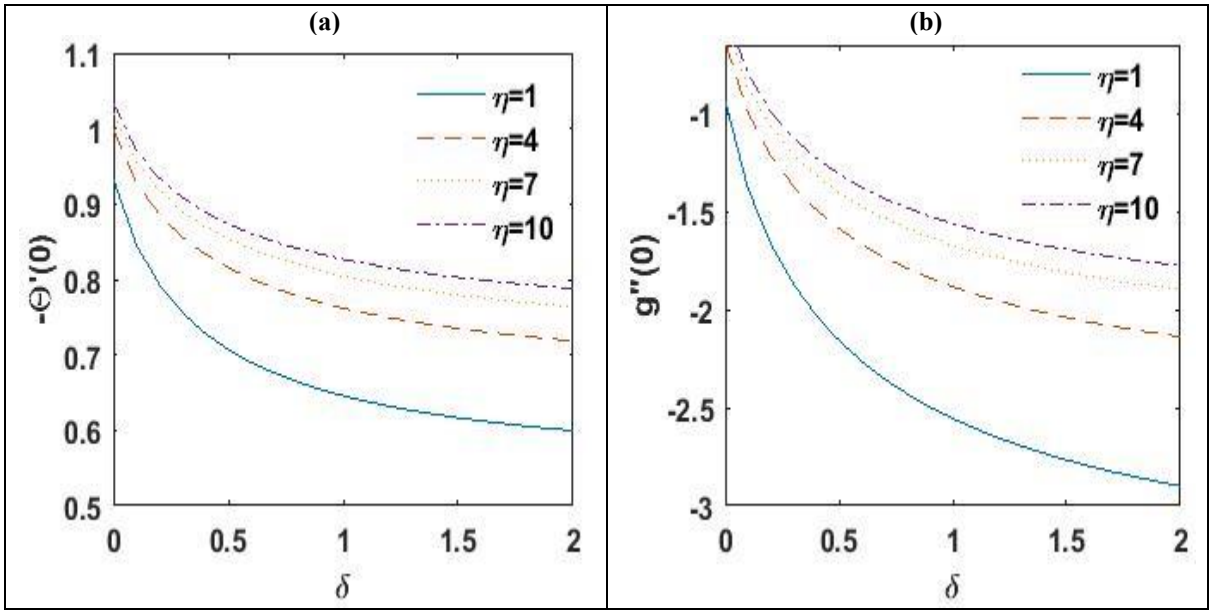

Figure 10. Impact of η on the (a) heat transfer rate and (b) skin friction.

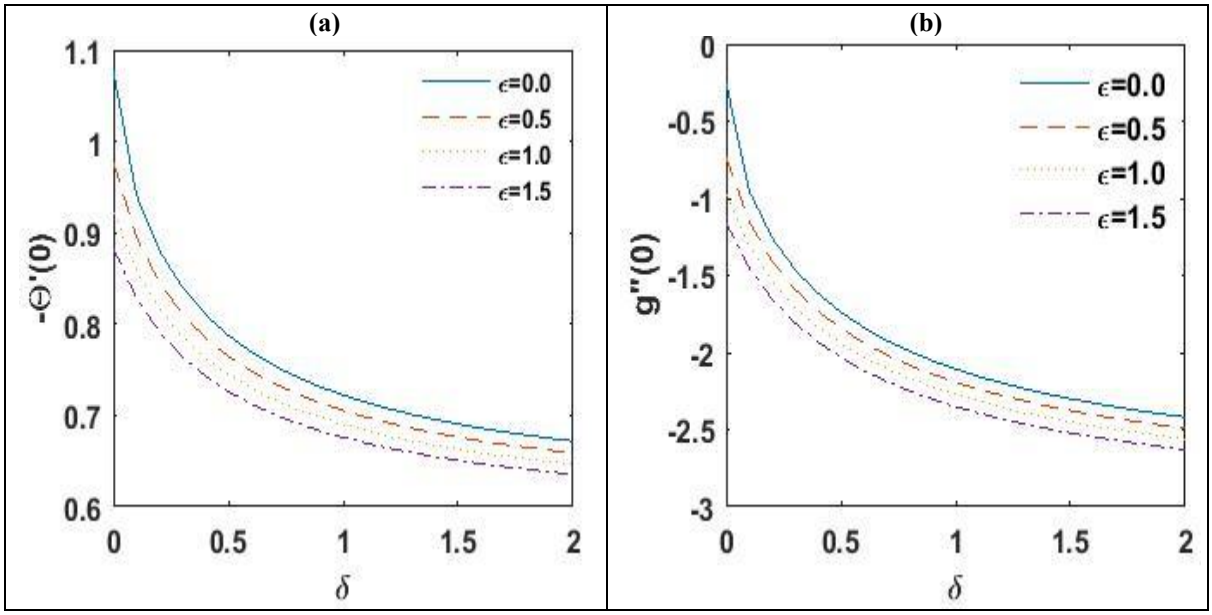

Figure 11. Impact of ε on the (a) heat transfer rate and (b) skin friction.

Fig 13 shows the impact of viscosity variation factor Q on the heat spread rate and skin friction. It is evident that an increase in the viscosity variation factor Q results in a reduction of the skin friction coefficient as well as the rate of heat transmission. This occurrence can be described as follows: as the viscosity variation factor Q upsurges, the effective viscosity of the fluid nearby the surface declines due to the converse connection amid viscosity and temperature. The lesser viscosity augments fluid mobility but diminishes the velocity gradient and convective heat transportation nearby the wall. As a result, both the wall shear stress and the temperature gradient lessening, prominent to poorer local skin friction and a reduced rate of heat transmission.

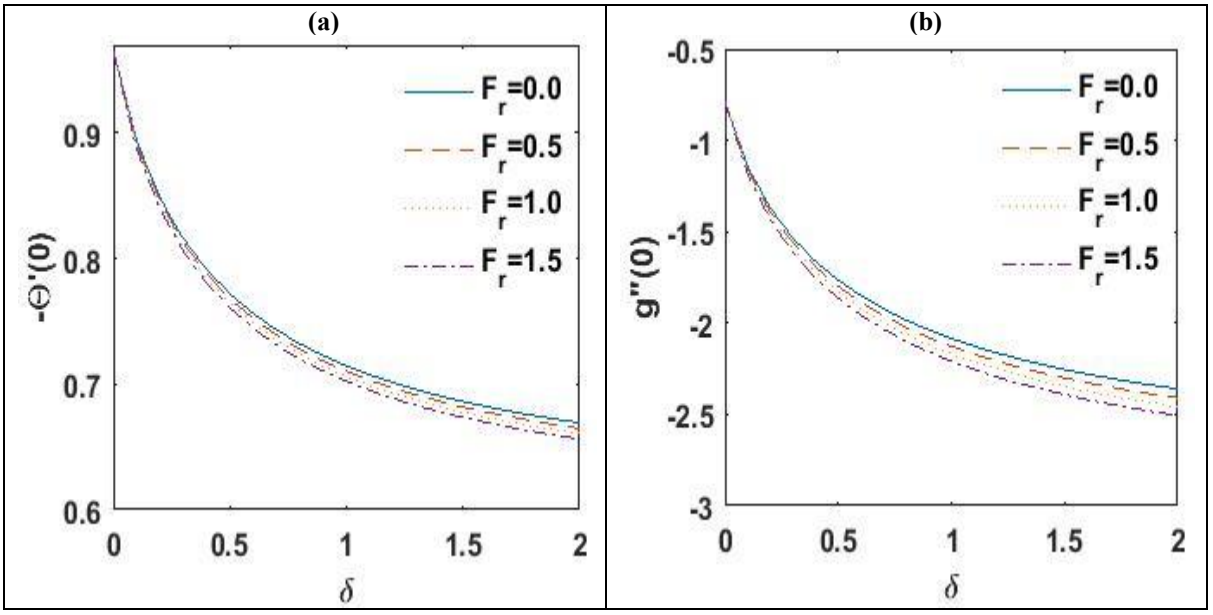

Figure 12. Impression of F_r on the (a) heat transfer rate and (b) skin friction.

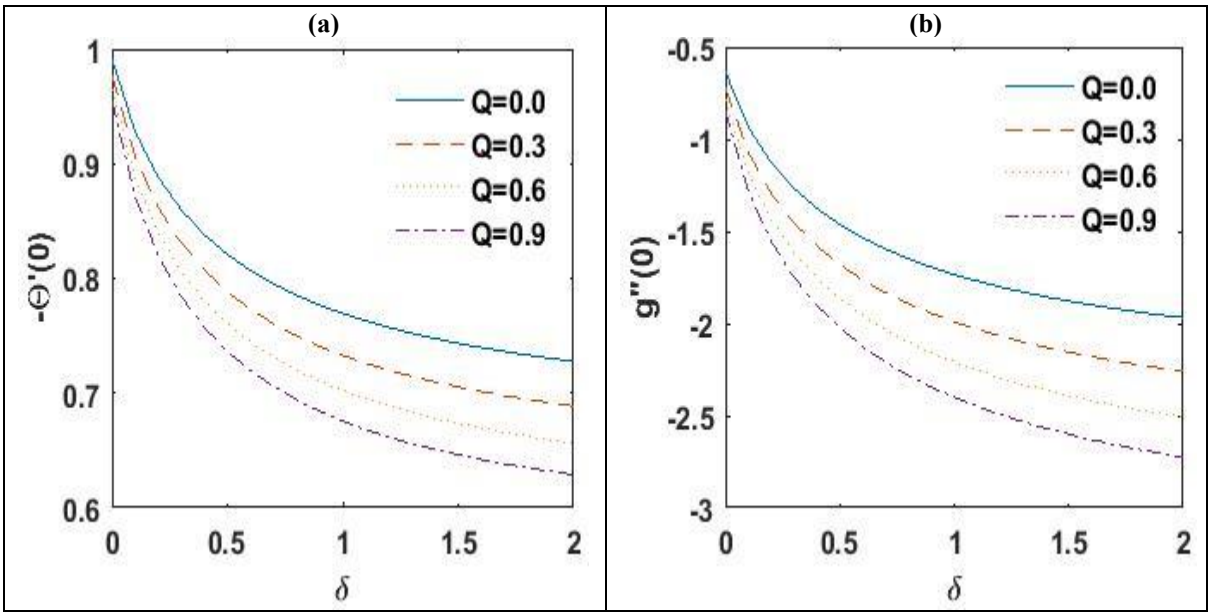

Figure 13. Impact of Q on the (a) heat transfer rate and (b) skin friction.

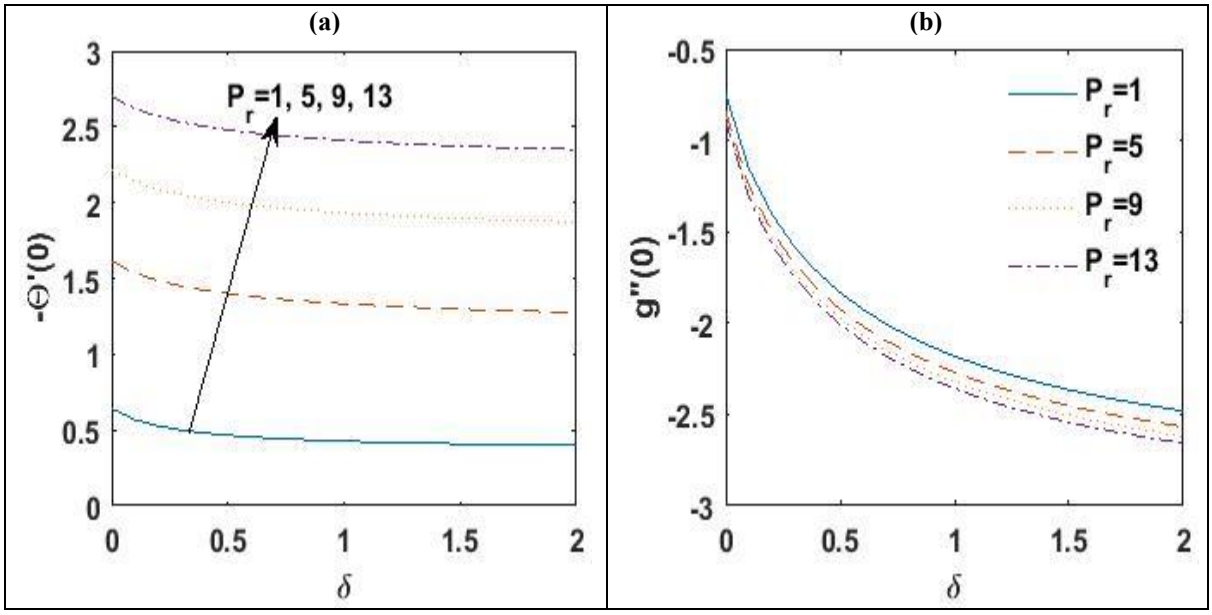

Figure 14. Impact of P_r on the (a) heat transfer rate and (b) skin friction.

Fig. 14 and Table 7 show the control of the Prandtl number P_r on the heat spread rate and skin friction. It is perceived that rising P_r leads to a rise in the heat spread rate, while the skin friction declines. Physically, a greater Prandtl number P_r relates to a liquid with poorer thermal diffusivity comparative to momentum diffusivity. This produces a thinner thermal boundary layer, which improves the temperature gradient at the wall and surges the heat transfer rate. At the same time, the thinner thermal boundary layer slightly reduces the velocity gradient near the wall, lowering the wall shear stress and, consequently, the skin friction.

5. Conclusion

This research presents a numerical investigation of the effects of key physical parameters on the velocity, temperature, skin friction, and heat transfer characteristics of a Casson fluid over a nonlinearly stretching sheet entrenched in a permeable medium, considering variable viscosity and the influence of a magnetic field. The governing boundary-layer equations were cracked applying the Runge–Kutta practice, with the solution confirmed by the MATLAB's bvp5c solver. The results were further validated against formerly published studies, displaying outstanding agreement. High accuracy was ensured through the use of stringent relative and absolute tolerances in the numerical scheme. The main outcomes of the study can be concise as follows:

- The velocity profile of the Casson fluid increases with higher Prandtl number P_r and greater the nonlinear factor of the stretching sheet η, but decreases with increasing the porosity factor ε, the Forchheimer number F_r, the Casson factor δ, the magnetic field factor M and the viscosity variation factor Q.
- The temperature profile drops with accumulating Prandtl number P_r and the nonlinear factor of the stretching sheet η, whereas it increases with higher the porosity factor ε, the Forchheimer number F_r, the Casson factor δ, the magnetic field factor M and the viscosity variation factor Q.
- An increase in the nonlinear factor of the stretching sheet η enhances both skin friction and heat transfer rate.
- Higher the porosity factor ε, Forchheimer number F_r, and viscosity variation factor Q reduce both skin friction and heat transfer rate.

- Cumulative the Prandtl number P_r raises the heat transfer rate while slightly decreasing skin friction.
- An upsurge in the magnetic field factor M or Casson factor δ declines both skin friction and heat transfer rate.

Funding Declaration

This research was supported by the University of Nizwa Grant No.: UoN/4/IF/2025, Nizwa, Oman.

References

[1] A. M. Mohamad, D. Yadav, M. K. Awasthi, R. Ragoju, M. Hassan, Heat and Mass Transfers on the Chemically Reactive Thermosolutal Convective Flow of Rivlin-Ericksen Fluid over a Porous Medium with Viscous Dissipation Effect, *Journal of Computational Applied Mechanics,* Vol. 56, No. 3, pp. 561-586, 2025.

[2] S. Abdul Gaffar, V. Ramachandra Prasad, E. Keshava Reddy, Computational study of Jeffrey's non-Newtonian fluid past a semi-infinite vertical plate with thermal radiation and heat generation/absorption, *Ain Shams Engineering Journal,* Vol. 8, No. 2, pp. 277-294, 2017/06/01/, 2017.

[3] M. K. Awasthi, A. K. Shukla, A. Kumar, N. Dutt, D. Yadav, *Chapter 10 - Instability of Casson fluid–viscous fluid interfaces*, in: H. M. Srivastava, G. Arora, F. A. Shah, *Advances in Computational Methods and Modeling for Science and Engineering*, Eds., pp. 113-121: Morgan Kaufmann, 2025.

[4] A. M. Mohamad, D. Yadav, M. K. Awasthi, R. Ragoju, A. Mahajan, M. Hassan, Influence of temperature reliant viscosity on the magnetohydrodynamic instability in a Navier–Stokes–Voigt fluid, *Multiscale and Multidisciplinary Modeling, Experiments and Design,* Vol. 9, No. 1, pp. 16, 2025/10/29, 2025.

[5] A. M. Mohamad, D. Yadav, M. K. Awasthi, R. Ragoju, K. Bhattacharyya, A. Mahajan, Analytical and numerical examinations on the stability investigation of Casson nanofluid flow in a permeable layer controlled by vertical throughflow, *World Journal of Engineering,* Vol. ahead-of-print, No. ahead-of-print, 2024.

[6] A. M. Mohamad, D. Yadav, S. Bharatharajan Nair, M. K. Awasthi, R. Ravi, K. Bhattacharyya, The effect of Péclet number on the onset of Casson fluid convective motion in a porous layer: Analytical and numerical investigations, *Numerical Heat Transfer, Part B: Fundamentals*, 2024.

[7] D. Yadav, S. B. Nair, M. K. Awasthi, R. Ragoju, K. Bhattacharyya, Linear and nonlinear investigations of the impact of chemical reaction on the thermohaline convection in a permeable layer saturated with Casson fluid, *Physics of Fluids,* Vol. 36, No. 1, pp. 014106, 2024.

[8] D. Yadav, M. K. Awasthi, A. K. Singh, R. Ravi, K. Bhattacharyya, U. S. Mahabaleshwar, Thermal boundary conditions and rotation effects on the onset of casson fluid convection in a permeable layer produced by purely interior heating, *Numerical Heat Transfer, Part B: Fundamentals,* Vol. 86, No. 12, pp. 4112-4126, 2025/12/02, 2025.

[9] M. Awais, T. Salahuddin, S. Muhammad, Evaluating the thermo-physical characteristics of non-Newtonian Casson fluid with enthalpy change, *Thermal Science and Engineering Progress,* Vol. 42, pp. 101948, 2023.

[10] N. S. Akbar, T. Muhammad, Physical aspects of electro osmotically interactive Cilia propulsion on symmetric plus asymmetric conduit flow of couple stress fluid with thermal radiation and heat transfer, *Scientific Reports,* Vol. 13, No. 1, pp. 18491, 2023.

[11] K. A. Khan, F. Jamil, J. Ali, I. Khan, N. Ahmed, M. Andualem, M. Rafiq, Analytical simulation of heat and mass transmission in casson fluid flow across a stretching surface, *Mathematical Problems in Engineering,* Vol. 2022, No. 1, pp. 5576194, 2022.

[12] V. K. Verma, S. Mondal, A brief review of numerical methods for heat and mass transfer of Casson fluids, *Partial Differential Equations in Applied Mathematics,* Vol. 3, pp. 100034, 2021.

[13] M. Aneja, A. Chandra, S. Sharma, Natural convection in a partially heated porous cavity to Casson fluid, *International Communications in Heat and Mass Transfer,* Vol. 114, pp. 104555, 2020/05/01/, 2020.

[14] K. Anantha Kumar, V. Sugunamma, N. Sandeep, Effect of thermal radiation on MHD Casson fluid flow over an exponentially stretching curved sheet, *Journal of Thermal Analysis and Calorimetry,* Vol. 140, No. 5, pp. 2377-2385, 2020.

[15] Y. D. Reddy, B. S. Goud, A. J. Chamkha, M. A. Kumar, Influence of radiation and viscous dissipation on MHD heat transfer Casson nanofluid flow along a nonlinear stretching surface with chemical reaction, *Heat Transfer,* Vol. 51, No. 4, pp. 3495-3511, 2022.

[16] T. Salahuddin, M. Arshad, N. Siddique, A. Alqahtani, M. Malik, Thermophyical properties and internal energy change in Casson fluid flow along with activation energy, *Ain Shams Engineering Journal,* Vol. 11, No. 4, pp. 1355-1365, 2020.

[17] M. Hamid, M. Usman, Z. H. Khan, R. Ahmad, W. Wang, Dual solutions and stability analysis of flow and heat transfer of Casson fluid over a stretching sheet, *Physics Letters A,* Vol. 383, No. 20, pp. 2400-2408, 2019/07/18/, 2019.

[18] M. Hamid, M. Usman, Z. H. Khan, R. U. Haq, W. Wang, Heat transfer and flow analysis of Casson fluid enclosed in a partially heated trapezoidal cavity, *International Communications in Heat and Mass Transfer,* Vol. 108, pp. 104284, 2019/11/01/, 2019.

[19] G. Ramesh, B. Prasannakumara, B. Gireesha, M. Rashidi, Casson fluid flow near the stagnation point over a stretching sheet with variable thickness and radiation, *Journal of Applied Fluid Mechanics,* Vol. 9, No. 3, pp. 1115-1022, 2016.

[20] M. Gnaneswara Reddy, M. Sudharani, K. Ganesh Kumar, A. J. Chamkha, G. Lorenzini, Physical aspects of Darcy–Forchheimer flow and dissipative heat transfer of Reiner–Philippoff fluid: MG Reddy et al, *Journal of Thermal Analysis and Calorimetry,* Vol. 141, No. 2, pp. 829-838, 2020.

[21] Q. Raza, X. Wang, Analyzing heat transfer behavior in two-dimensional Darcy–Forchheimer porous medium using magnetized nanoparticles, *Numerical Heat Transfer, Part B: Fundamentals*, pp. 1-21, 2024.

[22] K. G. Kumar, A. J. Chamkha, Darcy-Forchheimer flow and heat transfer of water-based Cu nanoparticles in convergent/divergent channel subjected to particle shape effect, *The European Physical Journal Plus,* Vol. 134, No. 3, pp. 107, 2019.

[23] D. Yadav, M. K. Awasthi, A. M. Mohamad, R. Ragoju, K. Bhattacharyya, M. Hassan, The onset of Casson fluid convection in a permeable medium layer produced by purely inner heating with magnetic field, *Journal of Computational Applied Mechanics,* Vol. 55, No. 3, pp. 340-354, 2024.

[24] A. J. Chamkha, Unsteady MHD convective heat and mass transfer past a semi-infinite vertical permeable moving plate with heat absorption, *International journal of engineering science,* Vol. 42, No. 2, pp. 217-230, 2004.

[25] A. Mythreye, J. Pramod, K. Balamurugan, Chemical reaction on unsteady MHD convective heat and mass transfer past a semi-infinite vertical permeable moving plate with heat absorption, *Procedia Engineering,* Vol. 127, pp. 613-620, 2015.

[26] N. Ahmed, S. Agarwalla, Effect of heat sink on transient MHD mass transfer flow past an accelerated vertical plate with chemical reaction, *Advances and Applications in Fluid Mechanics,* Vol. 19, No. 2, pp. 273, 2016.

[27] K. Choudhury, N. Ahmed, Soret effect on transient MHD convective flow past a semi-infinite vertical porous plate with heat sink and chemical reaction, *Applications and Applied Mathematics: An International Journal (AAM),* Vol. 13, No. 2, pp. 15, 2018.

[28] S. Naramgari, S. Vangala, M. Penem, Aligned magnetic field, radiation, and rotation effects on unsteady hydromagnetic free convection flow past an impulsively moving vertical plate in a porous medium, *International journal of engineering mathematics,* Vol. 2014, No. 1, pp. 565162, 2014.

[29] L. Manjula, R. Muthucumaraswamy, Heat and mass transfer effect on an infinite vertical plate in the presence of hall current and thermal radiation with variable temperature, *International Journal of Applied Mechanics and Engineering,* Vol. 26, No. 3, 2021.

[30] S. Ghosh, S. Mukhopadhyay, Unsteady MHD three-dimensional flow of nanofluid over a stretching surface with zero nanoparticles flux and thermal radiation, *Waves in Random and Complex Media,* Vol. 34, No. 4, pp. 2637-2653, 2024.

[31] R. Kodi, O. Mopuri, S. Sree, V. Konduru, Investigation of MHD Casson fluid flow past a vertical porous plate under the influence of thermal diffusion and chemical reaction, *Heat Transfer,* Vol. 51, No. 1, pp. 377-394, 2022.

[32] C. P. Kumar, K. Raghunath, M. Obulesu, Thermal diffusion and inclined magnetic field effects on MHD free convection flow of Casson fluid past an inclined plate in conducting field, *Turkish Journal of Computer and Mathematics Education,* Vol. 12, No. 13, pp. 960-977, 2021.

[33] M. M. Rashidi, S. A. Mohimanian pour, S. Abbasbandy, Analytic approximate solutions for heat transfer of a micropolar fluid through a porous medium with radiation, *Communications in Nonlinear Science and Numerical Simulation,* Vol. 16, No. 4, pp. 1874-1889, 2011/04/01/, 2011.

[34] M. Ziaul Haque, M. Mahmud Alam, M. Ferdows, A. Postelnicu, Micropolar fluid behaviors on steady MHD free convection and mass transfer flow with constant heat and mass fluxes, joule heating and viscous dissipation, *Journal of King Saud University - Engineering Sciences,* Vol. 24, No. 2, pp. 71-84, 2012/07/01/, 2012.

[35] K. Bhattacharyya, S. Mukhopadhyay, G. C. Layek, I. Pop, Effects of thermal radiation on micropolar fluid flow and heat transfer over a porous shrinking sheet, *International Journal of Heat and Mass Transfer,* Vol. 55, No. 11, pp. 2945-2952, 2012/05/01/, 2012.

[36] M. Sheikholeslami, M. Hatami, D. D. Ganji, Micropolar fluid flow and heat transfer in a permeable channel using analytical method, *Journal of Molecular Liquids,* Vol. 194, pp. 30-36, 2014/06/01/, 2014.

[37] D. Bhukta, G. Dash, S. Mishra, Heat and mass transfer on MHD flow of a viscoelastic fluid through porous media over a shrinking sheet, *International Scholarly Research Notices,* Vol. 2014, No. 1, pp. 572162, 2014.

[38] I. Pop, R. S. R. Gorla, M. Rashidi, The effect of variable viscosity on flow and heat transfer to a continuous moving flat plate, *International Journal of Engineering Science,* Vol. 30, No. 1, pp. 1-6, 1992/01/01/, 1992.

[39] E. M. A. Elbashbeshy, M. A. A. Bazid, The effect of temperature-dependent viscosity on heat transfer over a continuous moving surface with variable internal heat generation, *Applied Mathematics and Computation,* Vol. 153, No. 3, pp. 721-731, 2004/06/14/, 2004.

[40] M. S. Abel, S. K. Khan, K. V. Prasad, Study of visco-elastic fluid flow and heat transfer over a stretching sheet with variable viscosity, *International Journal of Non-Linear Mechanics,* Vol. 37, No. 1, pp. 81-88, 2002/01/01/, 2002.

[41] M. E. Ali, The effect of variable viscosity on mixed convection heat transfer along a vertical moving surface, *International Journal of Thermal Sciences,* Vol. 45, No. 1, pp. 60-69, 2006.

[42] N. Eldabe, G. Saddeck, A. El-Sayed, Heat transfer of MHD non-Newtonian Casson fluid flow between two rotating cylinders, *Mechanics and Mechanical Engineering,* Vol. 5, No. 2, pp. 237-251, 2001.

[43] S. Mukhopadhyay, P. R. De, K. Bhattacharyya, G. C. Layek, Casson fluid flow over an unsteady stretching surface, *Ain Shams Engineering Journal,* Vol. 4, No. 4, pp. 933-938, 2013/12/01/, 2013.

[44] M. Devi, U. Gupta, Stability analysis of binary Casson nanofluid convection with viscosity and conductivity variations using Darcy–Brinkman model, *Journal of Heat Transfer,* Vol. 144, No. 12, pp. 121201, 2022.

[45] O. Makinde, M. Gnaneswara Reddy, MHD peristaltic slip flow of Casson fluid and heat transfer in channel filled with a porous medium, *Scientia Iranica,* Vol. 26, No. 4, pp. 2342-2355, 2019.

[46] H. T. Malik, M. Farooq, S. Ahmad, M. M. Ibrahim Mohamed, Convective heat transportation in exponentially stratified Casson fluid flow over an inclined sheet with viscous dissipation, *Case Studies in Thermal Engineering,* Vol. 52, pp. 103720, 2023/12/01/, 2023.

[47] D. Thenmozhi, M. Eswara Rao, R. L. V. Renuka Devi, C. Nagalakshmi, Analysis of Jeffrey fluid on MHD flow with stretching – porous sheets of heat transfer system, *Forces in Mechanics,* Vol. 11, pp. 100180, 2023/05/01/, 2023.

[48] N. B, N. Kishan, J. V. Tawade, P. Meenapandi, B. Abdullaeva, M. Waqas, M. Gupta, N. Batool, F. Ahmad, Analysis of boundary layer flow of a Jeffrey fluid over a stretching or shrinking sheet immersed in a porous medium, *Partial Differential Equations in Applied Mathematics,* Vol. 12, pp. 100951, 2024/12/01/, 2024.

[49] S. S. Benal, J. V. Tawade, M. M. Biradar, H. L. Allasi, Effects of the magnetohydrodynamic flow within the boundary layer of a jeffery fluid in a porous medium over a shrinking/stretching sheet, *Mathematical Problems in Engineering,* Vol. 2022, No. 1, pp. 7326504, 2022.

[50] O. D. Makinde, Second law analysis for variable viscosity hydromagnetic boundary layer flow with thermal radiation and Newtonian heating, *Entropy,* Vol. 13, No. 8, pp. 1446-1464, 2011.

[51] F. Lai, F. Kulacki, The effect of variable viscosity on convective heat transfer along a vertical surface in a saturated porous medium, *International journal of heat and mass transfer,* Vol. 33, No. 5, pp. 1028-1031, 1990.

[52] F. Mabood, N. Pochai, Analytical investigation of magnetohydrodynamic flow over a nonlinear porous stretching sheet, *Advances in Mathematical Physics,* Vol. 2016, No. 1, pp. 7821405, 2016.

[53] K. Jabeen, M. Mushtaq, R. Akram, Analysis of the MHD boundary layer flow over a nonlinear stretching sheet in a porous medium using semianalytical approaches, *Mathematical Problems in Engineering,* Vol. 2020, No. 1, pp. 3012854, 2020.

[54] N. Alessa, R. Sindhu, S. Divya, S. Eswaramoorthi, K. Loganathan, K. S. Prasad, Computational Analysis of Darcy–Forchheimer Flow of Cu/Al–Al2O3 Hybrid Nanofluid in Water over a Heated Stretchable Plate with Nonlinear Radiation, *Micromachines,* Vol. 14, No. 2, pp. 338, 2023.

[55] P. Rana, R. Bhargava, Flow and heat transfer of a nanofluid over a nonlinearly stretching sheet: A numerical study, *Communications in Nonlinear Science and Numerical Simulation,* Vol. 17, No. 1, pp. 212-226, 2012/01/01/, 2012.

[56] D. Yadav, M. K. Awasthi, R. Ragoju, K. Bhattacharyya, A. Mahajan, J. Wang, Impact of viscous dissipation, throughflow and rotation on the thermal convective instability of Jeffrey fluid in a porous medium layer, *European Journal of Mechanics - B/Fluids,* Vol. 109, pp. 55-65, 2025/01/01/, 2025.

[57] D. Yadav, M. K. Awasthi, R. Ragoju, K. Bhattacharyya, R. Kodi, M. Hassan, J. Wang, Impact of temperature-reliant thermal conductivity and viscosity variations on the convection of Jeffrey fluid in a rotating cellular porous layer, in *Proceeding of,* The Royal Society, pp. 20240206.

[58] G. Rasool, A. Shafiq, C. M. Khalique, T. Zhang, Magnetohydrodynamic Darcy–Forchheimer nanofluid flow over a nonlinear stretching sheet, *Physica Scripta,* Vol. 94, No. 10, pp. 105221, 2019/08/08, 2019.

[59] M. Jawad, M. K. Hameed, K. S. Nisar, A. H. Majeed, Darcy-Forchheimer flow of maxwell nanofluid flow over a porous stretching sheet with Arrhenius activation energy and nield boundary conditions, *Case Studies in Thermal Engineering,* Vol. 44, pp. 102830, 2023/04/01/, 2023.

[60] C. Liu, M. U. Khan, M. Ramzan, Y.-M. Chu, S. Kadry, M. Y. Malik, R. Chinram, Nonlinear radiative Maxwell nanofluid flow in a Darcy–Forchheimer permeable media over a stretching cylinder with chemical reaction and bioconvection, *Scientific Reports,* Vol. 11, No. 1, pp. 9391, 2021/04/30, 2021.

[61] S. Manjunatha, J. S. Kumar, S. V. K. Varma, Impacts of heat generation and Buoyancy forces on hyperbolic Tangent Magneto ferrofluid flow with Darcy–Forchheimer model over a nonlinear stretching sheet: RSM analysis, *The European Physical Journal Plus,* Vol. 140, No. 6, pp. 577, 2025/06/24, 2025.

[62] S. Pramanik, Casson fluid flow and heat transfer past an exponentially porous stretching surface in presence of thermal radiation, *Ain Shams Engineering Journal,* Vol. 5, No. 1, pp. 205-212, 2014/03/01/, 2014.

[63] D. Yadav, M. K. Awasthi, R. Ragoju, K. Bhattacharyya, R. Kodi, J. Wang, The impact of rotation on the onset of cellular convective movement in a casson fluid saturated permeable layer with temperature dependent thermal conductivity and viscosity deviations, *Chinese Journal of Physics,* Vol. 91, pp. 262-277, 2024/10/01/, 2024.

[64] D. D. Ganji, H. Bararnia, S. Soleimani, E. Ghasemi, ANALYTICAL SOLUTION OF THE MAGNETO-HYDRODYNAMIC FLOW OVER A NONLINEAR STRETCHING SHEET, *Modern Physics Letters B,* Vol. 23, No. 20n21, pp. 2541-2556, 2009/08/20, 2009.

[65] T. Hayat, Q. Hussain, T. Javed, The modified decomposition method and Padé approximants for the MHD flow over a non-linear stretching sheet, *Nonlinear Analysis: Real World Applications,* Vol. 10, No. 2, pp. 966-973, 2009/04/01/, 2009.

[66] M. M. Nandeppanavar, Flow and Heat Transfer Analysis of Casson Fluid due to A Stretching Sheet: An Analytical Solution, *Advances in Physics theories and Applications,* Vol. 50, pp. 2224-2225, 2015.

[67] R. Cortell, Viscous flow and heat transfer over a nonlinearly stretching sheet, *Applied Mathematics and Computation,* Vol. 184, No. 2, pp. 864-873, 2007/01/15/, 2007.